Electromagnetically controlled multiferroic thermal diode

Electromagnetically controlled multiferroic thermal diode

L. Chotorlishvili, S. R. Etesami, and J. Berakdar
Institut für Physik, Martin-Luther-Universität Halle-Wittenberg, 06099 Halle/Saale, Germany

R. Khomeriki
Physics Department, Tbilisi State University, 0128 Tbilisi, Georgia

Jie Ren
Center for Phononics and Thermal Energy Science, School of Physics Science and Engineering, Tongji University, 200092 Shanghai, China and Department of Chemistry, Massachusetts Institute of Technology, 77 Massachusetts Avenue, Cambridge, Massachusetts 02139, USA
(Received 10 March 2015; revised manuscript received 28 September 2015; published 30 October 2015)

We propose an electromagnetically tunable thermal diode based on a two-phase multiferroic composite. Analytical and full numerical calculations for a prototypical heterojunction composed of iron on barium titanate in the tetragonal phase demonstrate a strong heat rectification effect that can be controlled externally by a moderate electric field. This finding is important for thermally based information processing and sensing and can also be integrated in (spin) electronic circuits for heat management and recycling.

DOI: 10.1103/PhysRevB.92.134424 PACS number(s): 44.10.+i, 05.20.−y, 05.60.−k, 66.70.−f

I. INTRODUCTION

A diode, i.e., a device that controls the electrical current flow direction, is an integral part of everyday electronics. The sonic counterpart governs the propagation of mechanical vibrations and has wide-ranging applications in acoustics, medical sensing, and heat management. Acoustic (sound waves) diodes were recently demonstrated [1,2]. Thermal diodes are more challenging, however. Even though heat and sound are of phononic nature, the frequency range of the latter is typically in the range of kilohertz to gigahertz (hypersound). Heat, on the other hand, is mediated by a broad spectrum of terahertz vibrations. Controlling heat diodes is therefore more delicate, but on the plus side the relevant scale for material structuring is the nanometer, therefore allowing us, as shown below, to exploit the marked achievements of nanotechnology in tuning the material compositions and the associated electric, magnetic, and optical properties. Applications are diverse. For instance, in spintronics it was shown that a thermal gradient may generate a direction-dependent spin current that can be utilized for information handling [3]. Such thermal magnetic diodes would add therefore an essential element towards thermally based spintronic circuits.

Generally, substantial research has been devoted in recent years to phononic-based diodes [4–8]. Our aim here is to add a different facet, namely, the external control of thermal diodes via electric and/or magnetic fields. In view of an experimental implementation we consider a well-tested system composed of a two-phase multiferroic (MF), i.e., a ferroelectric (FE) structure interfacially coupled to a ferromagnet (FM). The interfacial coupling changes the transmission and conversion of magnetic excitations into ferroelectric ones. The thermal energy in the proposed multiferroic thermal diode is carried by elementary excitations of electric polarization and magnetization (rather than by vibrational excitation in a conventional thermal diode), both of which are susceptible to external electric or magnetic fields. As shown below, the performance of the thermal diode is then controllable electromagnetically. Multiferroics, in general, are intensively investigated in view of a variety of applications in electronics and sensing [9–18]. Thus, the current study augments these applications with the possibility of a controlled heat recycling.

II. MULTIFERROIC THERMAL DIODE

The physics of a thermal diode is a resonance phenomenon [8] relying on the overlapping of the temperature-dependent power spectra of thermal excitations (mediated by polarization, magnetization, and other types of excitations) of the two different diode segments. In addition, the dependence of frequency on the oscillation amplitude, i.e., the nonlinear nature of excitations, is a key factor. A perfect thermal conductance hints at power spectra overlapping. Our aim here is to demonstrate that thermal bias applied on the edges of a MF thermal diode generates a heat flux that can be rectified and controlled by temperature, electric field, and interface ME coupling. To this end, we assume that the FM part of the thermal diode is a normal ferromagnetic metal (e.g., Fe). As a prototypical FE we employ $BaTiO_3$. For this experimentally realized composite an interfacial magnetoelectric coupling [14,19,20] was demonstrated. The ferroelectric dynamics of $BaTiO_3$ is captured by the Ginzburg-Landau-Devonshire (GLD) potential [21] valid at temperatures $\sim 280-400$ K (tetragonal phase) in which case the polarization switches bidirectionally. In the spirit of a coarse-grained approach, the FE order parameter is discretized into N cells (also called sites), each with a size of 1 nm [22]. The coarse-grained polarization at site n is referred by p_n. In the tetragonal phase, realized also at room temperature, we have one component (Ising-type) polarization vector $\vec{p}_n = (0,0,p_n^z)$, $n = 1,\ldots,N$ (here n is the site number) entering the ferroelectric free-energy functional [21]. In the context of a thermal diode an important fact is that, by applying an external electric field, the temperature range of the tetragonal phase can be extended [23,24]. Taking the general cubic paraelectric phase as a reference, we performed numerical calculations which

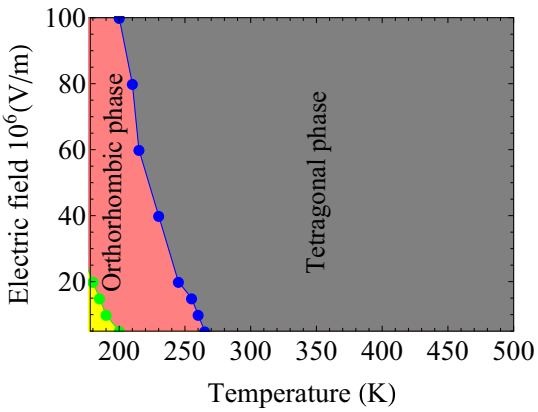

FIG. 1. (Color online) Full simulations of the $BaTiO_3$ phase diagram based on the eight-order temperature-dependent potential [23].

turned out to be in line with the experimentally determined phase diagram [23]. The result of our calculations is shown in Fig. 1. As we see by applying an electric field with an amplitude $E = 100$ MV/m, the lower limit of the tetragonal phase is reduced from $T = 280$ K to $T = 200$ K, while the upper limit of the tetragonal phase exceeds $T = 500$ K.

For FM we employ the well-established classical Heisenberg model to describe transversal excitations of the coupled (coarse-grained) magnetic moment $\vec{M}_n$ at site n. Experiments done for different materials [25] show the dominant role of magnons for the thermal heat conductance at relatively high temperatures $T > 20$ K. The relevance of magnons to thermal heat conductance was also confirmed by the spin Seebeck effect [26]. The multiferroic interaction between the interfacial FE cell (with p_N) and the adjacent FM cell (with M^z_{N+1}) is described by the $\mathcal{PT}$-invariant term $V_{\mathrm{ME},m} = -g_m(p_N M^z_{N+1})^m$, the form and the origin of which we discussed at length recently and contrasted with experimental findings [27–34]. Here we account for the linear ($V_{\mathrm{ME},1}$) and quadratic ($V_{\mathrm{ME},2}$) terms (for low-energy excitations, higher-order terms are less relevant to the effects studied here). g_m is the magnetoelectric coupling constant. The total Hamiltonian of the composite reads $H = H_p + H_s + V_{\mathrm{ME}}$, where $H_p = \sum_{n=1}^{N}[\frac{1}{2}(\frac{dp_n}{dt})^2 - \frac{\alpha^{\mathrm{EF}}}{2}p_n^2 + \frac{\beta^{\mathrm{EF}}}{4}p_n^4 + \frac{1}{2}(p_{n+1}-p_n)^2 - Ep_n]$ is the FE Hamiltonian and $H_S = \sum_{k=N+1}^{M}[-J\vec{M}_k\vec{M}_{k+1} - D(M^z_k)^2 - BM^z_k]$ is the FM Hamiltonian. Unless otherwise stated, we use dimensionless units (d.u.). For values of all parameters in conventional units as used experimentally, we refer to the Appendix. The effect of the applied thermal bias can be described by a stochastic field added to the effective electric field in the time-dependent GLD equation [35]. The microscopic mechanism for the emergence of noise in FE is based on phonons. Thermally activated phonons lead to electric dipole vibrations that can be captured by a random electric field. Experimentally, thermally activated polarization switches at much lower field strengths than predicted by GLD phenomenology [36] (without including noise). The equations of motion for the polarization p_n read [34]

$$\begin{aligned}\frac{dp_n}{dt} &= q_n,\\ \frac{dq_n}{dt} &= \alpha^{\mathrm{FE}}p_n - \beta^{\mathrm{FE}}p_n^3 - (2p_n - p_{n+1} - p_{n-1}) + E\\ &\quad + g_1 M^z_1\delta_{nN} + 2g_2 p_n\left(M^z_1\right)^2\delta_{nN} - \gamma_n q_n\delta_{1n}\\ &\quad + \delta_{1n}\xi_n, \qquad n = 1,\ldots,N. \end{aligned} \tag{1}$$

Here α^{FE}, β^{FE} are the kinetic parameters of the GLD potential, E is the amplitude of the external electric field, $g_1 M^z_1\delta_{nN} + 2g_2 p_n(M^z_1)^2\delta_{nN}$ is the contribution from the ME coupling, and the last two terms in (1) describe the influence of the thermal bias applied on the edges of the FE chain. The correlation function of the random noise ξ_n is related to the kinetic constant γ_n and the thermal energy $k_B T$ via the Einstein relation

$$\langle\xi_m(t)\xi_m(t')\rangle = 2\gamma_m T_m\delta(t-t'), \quad m = 1,\ldots,N. \tag{2}$$

The magnetization dynamics of the FM part is governed by a set of coupled polarization-dependent LLG equations as follows:

$$\frac{d\vec{M}_k}{dt} = -\frac{1}{1+\alpha_k^2}\vec{M}_k \times \left(\vec{B}_k^{\mathrm{eff}} + \alpha_k\vec{M}_k \times \vec{B}_k^{\mathrm{eff}}\right). \tag{3}$$

Here $\alpha_k = \alpha\delta_{kM}$ and $\vec{B}_k^{\mathrm{eff}}$ are the total effective (electric polarization-dependent) magnetic field acting on the kth magnetic moment $k \in [N+1, M]$,

$$\begin{aligned}\vec{B}_k^{\mathrm{eff}} &= \vec{i}_z B + J(\vec{M}_{k-1} + \vec{M}_{k+1}) + \vec{i}_z 2DM^z_k\\ &\quad + \vec{i}_z g_1 p_N\delta_{k\,N+1} + \vec{i}_z 2g_2 p_N^2 M^z_k\delta_{k\,N+1} + \delta_{kM}\vec{\eta}_k. \end{aligned} \tag{4}$$

$\vec{i}_z$ is a unit vector along the magnetization direction of the undistorted FM which we choose as the z direction. The effective magnetic field [Eq. (4)] contains a deterministic contribution from the external magnetic field $\vec{i}_z B$ and the contributions from exchange $J(\vec{M}_{k-1} + \vec{M}_{k+1})$ and magnetic anisotropy $\vec{i}_z 2DM^z_k$. Due to its interfacial nature the magnetoelectric coupling $\vec{i}_z g_1 p_N\delta_{k\,N+1} + \vec{i}_z 2g_2 p_N^2 M^z_k\delta_{k\,N+1}$ acts on only the interfacial FM and FE cells. The random magnetic field $\vec{\eta}_k$ enters the dynamic of only the edge cells (thermal bias is applied at the end of the FM chain), while the heat propagation through the structure is evaluated self-consistently. The random magnetic field $\vec{\eta}_k$ is quantified via the correlation function

$$\left\langle\eta_k^i(t)\eta_k^j(t')\right\rangle = 2\alpha_k T_k\delta_{ij}\delta(t-t'). \tag{5}$$

Here i and j define the Cartesian components of the random magnetic field, k numbers the cell, and T_k is the cell-dependent local temperature. α_k is the dimensionless Gilbert damping constant. Values of the FM and FE parameters used in the calculations are given in Table I in the Appendix. Following the continuity equation for the local energy and the equipartition theorem, the heat current and the temperature profile can be evaluated self-consistently [8]. In particular, the expression for the heat current in the FE part reads $J_k^H = -\langle\dot{p}_k(p_{k+1} - p_k)\rangle$. The time derivative of the polarization $\dot{p}_k$ plays the role of a canonical momentum. In the FE part the local (site-dependent) temperature follows from its relation to the average

TABLE I. Parameters of an unstrained bulk $BaTiO_3$ single crystal [30,46] and bulk bcc Fe [31].

Parameter	SI units	Dimensional unit (d.u.)
	Bulk $BaTiO_3$ single crystal	
P_0	$0.265\,\mathrm{C/m^2}$	$p_n = P_n/P_0$
α_1	2.770×10^7 V m/C	$\alpha^{\mathrm{FE}} = \frac{\alpha_1}{\kappa} \approx 0.213$
α_2	$1.7 \times 10^8\,\mathrm{Vm^5/C^3}$	$\beta^{\mathrm{FE}} = \frac{\alpha_2 P_0^2}{\kappa} \approx 0.0918$
γ_v	2.5×10^{-5} V m s/C	$\gamma_m = \frac{\gamma_v \omega_0}{\kappa} \approx 0.192$
a_{FE}	1.02×10^{-9} m	
κ	1.3×10^8 V m/C	1
E	parameter (V/m)	$E \to \frac{1}{\kappa P_0} E \approx 3.4 \times 10^7 E$
T	parameter (K)	$T \to \frac{k_B}{\kappa P_0^2 a_{\mathrm{FE}}^3} T \approx 1.4 \times 10^{-3} T$
J	joules/s	$J \to \frac{1}{\kappa P_0^2 \omega_0 a_{\mathrm{FE}}^3} J \approx 10^8 J$
	Bulk bcc Fe	
M_S	1.71×10^6 A/m	$\vec{s}_k = \vec{M}_k/M_S = (\vec{S}_k/S)$
γ	$1.76 \times 10^{11}\,(\mathrm{T\,s})^{-1}$	
a_{FM}	1.0×10^{-9} m	
$\mu_S = M_S a_{\mathrm{FM}}^3$	1.71×10^{-21} J/T	
α_{FM}	1.0	
K_1	$2.0 \times 10^6\,\mathrm{J/m^3}$	$D = \frac{\gamma a_{\mathrm{FM}}^3 K_1}{\omega_0 \mu_S} = 0.206$
A	2.1×10^{-11} J/m	$J = \frac{\gamma a_{\mathrm{FM}} A}{\omega_0 \mu_S} = 2.16$
B	parameter (T)	$B \to \frac{\gamma}{\omega_0} B \approx 0.17 B$
T	parameter (K)	$T \to \frac{k_B \gamma}{\omega_0 \mu_S} T \approx 1.4 \times 10^{-3} T$
J	joules/s	$J \to \frac{\gamma}{\omega_0^2 \mu_S} J \approx 10^8 J$

local kinetic energy [8], which in our scaled units implies $T_k = \left(\frac{dp_k}{dt}\right)^2$. We note that here average means the long-time average, which in numerical simulations is implemented as the ensemble average. We derive the expression for the local heat current in the FM part by using the Heisenberg equation of motion $\frac{\partial h_{k,k+1}}{\partial t} = i[H_S, h_{k,k+1}]$. Here $H_S = -J \sum_k \vec{M}_k \cdot \vec{M}_{k+1} - D \sum_k (M_k^z)^2 - B \sum_k M_k^z$ is the Hamiltonian of the system, and $h_{k,k+1} = -J \vec{M}_k \cdot \vec{M}_{k+1} - D(M_k^z)^2 - B M_k^z$ is the local Hamiltonian. After straightforward calculations the heat current in the FM part is obtained as

$$\begin{aligned} J_k^H &= i[h_{k+1,k}, h_{k,k-1}] \\ &= 2DJ\left(M_{k+1}^x M_k^y M_k^z - M_k^x M_{k+1}^y M_k^z\right) \\ &\quad + DB\left(M_k^y M_{k+1}^x - M_k^x M_{k+1}^y\right) \\ &\quad - J^2\left(M_{k-1}^x M_k^y M_{k+1}^z - M_{k-1}^x M_{k+1}^y M_k^z\right) \\ &\quad - J^2\left(M_{k+1}^x M_{k-1}^y M_k^z - M_k^x M_{k-1}^y M_{k+1}^z\right) \\ &\quad - J^2\left(M_k^x M_{k+1}^y M_{k-1}^z - M_{k+1}^x M_k^y M_{k-1}^z\right). \end{aligned} \tag{6}$$

The equilibrium temperature T_k is evaluated self-consistently via the relation $M_k^{\parallel} = L\left(\frac{\vec{M}_k \cdot \vec{B}_k^{\mathrm{eff}}}{T_k}\right)$, where $L(\cdots)$ is the Langevin function and $M_k^{\parallel}$ is the component of the magnetization vector parallel to the effective field $\vec{B}_k^{\mathrm{eff}}$.

III. INTERFACE EFFECT AND HEAT RECTIFICATION

An important element of the thermal diode is the interface thermal resistance (ITR), usually referred to as the asymmetric Kapitza resistance [8] as it quantifies the asymmetry in interfacial resistance. We will consider the cases in which the hot thermal bath is applied to the FE part $T_{\mathrm{FE}} > T_{\mathrm{FM}}$ and to the FM part $T_{\mathrm{FE}} < T_{\mathrm{FM}}$. Inverting the sign of the thermal bias for a constant temperature difference $\Delta T = \mid T_{\mathrm{FE}} - T_{\mathrm{FM}} \mid$ drastically changes the heat flux $J_+ \neq J_-$ and the resistance $R_+ = \Delta T/J_+$, $R_- = \Delta T/J_-$. The ratio between the two different resistances R_+/R_- measures the rectification effect. The rectification effect of the MF diode stems from the overlapping of the spectra of the FE and FM subsystems. The frequency of the linear excitations in FM ω_{FM} is set by the anisotropy constant $\approx 2D$ [34]. The applied electric field substantially modifies the frequency of linear excitations in the FE part, ω_{FE}. Basically, the electric field shifts the minimum of the GLD potential derived from the relation $\partial_p H_p = 0$. In the limit of weak coupling between the dipoles, FE frequency takes the form $\omega_{\mathrm{FE}}(E) = \{4\alpha^{\mathrm{FE}} \cos^2[\cos^{-1}(\frac{3|E|}{2\alpha^{\mathrm{FE}}}\sqrt{\frac{3\beta^{\mathrm{FE}}}{\alpha^{\mathrm{FE}}}})/3] - \alpha^{\mathrm{FE}}\}^{1/2}$. So the correction in the FE frequency $\Delta\omega_{\mathrm{FE}} = \omega_{\mathrm{FE}}(E) - \omega_{\mathrm{FE}}(0)$ is even in the electric field (for more details we refer to the Appendix). Therefore, the heat current is symmetric with respect to the change of the electric field's sign $E \to -E$. On the other hand, maximal heat conductance occurs when FM and FE frequencies $\omega_{\mathrm{FM}} \approx \omega_{\mathrm{FE}}(0) + \Delta\omega_{\mathrm{FE}}$ match. Thus, the electric field can be utilized to enhance the heat current. From the frequency-matching condition and for the parameters listed in Table I in the Appendix, we obtain an estimation of the optimum electric field as $|E| = |\frac{2\alpha^{\mathrm{FE}}}{3}\sqrt{\frac{\alpha^{\mathrm{FE}}}{3\beta^{\mathrm{FE}}}} \cos[\frac{3}{2}\cos^{-1}(\frac{4D^2 - \alpha^{\mathrm{FE}}}{2\alpha^{\mathrm{FE}}})]| = 0.1$ (d.u.). In conventional units this corresponds to an electric field of $E = 3.4 \times 10^4$ V/cm. Increasing the electric field strength results in a mismatch of FE and FM spectra and hence a decrease of the heat current. This analytical estimation is confirmed by full numerical calculations as well (Fig. 3 below). Interface ME coupling leads to a small shift between analytically estimated and numerically calculated values of the optimum electric field. However, we see a prominent maximum in the heat current for optimal electric field.

IV. TEMPERATURE EFFECTS ON MF DIODE

We implemented full numerical simulations for a MF thermal diode consisting of 50 dipolar and 50 magnetic cells. Calculations are also done for a larger system (not shown) up to 500 dipolar and 500 magnetic cells, and we did not observe significant size effects. Of special interest is the rectification effect. We present the edge temperatures in the following form: $T_1 = T_0 + T_S\Delta$, $T_M = T_0 - T_S\Delta$, where M is the total number of sites. Thus, the difference between the edges temperatures is $T_1 - T_M = 2T_S\Delta$. Inverting the thermal bias simply means $\Delta \to -\Delta$. The heat current as a function of Δ for different values of T_0 is shown in Fig. 2(a). We observe that at larger temperature T_0 the asymmetry becomes stronger. The uniform heat flux through the system [see Fig. 2(b)] affirms that the system is in the nonequilibrium steady state. On the other hand, due to the different heat capacities of the FE and FM systems and the different heat exchange rates with the environment, the temperatures formed self-consistently in the FE and FM parts are different. In the case of an applied positive thermal bias the heat flux $J_+ = 0.8$ d.u., while for a negative

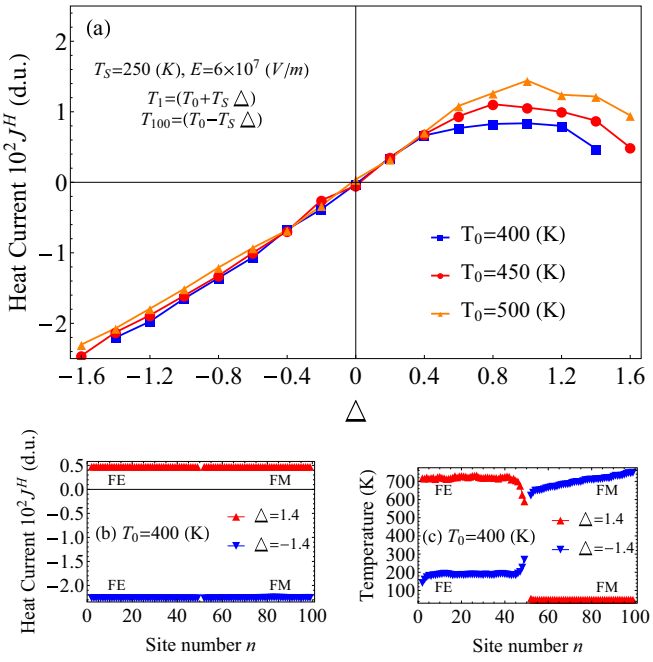

FIG. 2. (Color online) (a) Diode heat current under different edge temperatures. The multiferroic diode includes 50 FE cells (from 1 to 50) and 50 FM cells (from 51 to 100). In dimensional units, the applied electric and magnetic fields are $E = 1.74$ d.u. and $B = 0.0$ d.u., and FE-FM coupling coefficients are $g_1 = g_2 = -1$ d.u. Other employed parameters and reduced unit coefficients are tabulated in Table I in the Appendix. (b) Heat current profile for forward temperature bias ($\Delta = 1.4$), reverse temperature bias ($\Delta = -1.4$), and $T_0 = 400$ K. (c) Temperature profiles for forward temperature bias ($\Delta = 1.4$) and reverse temperature bias ($\Delta = -1.4$), $T_0 = 400$ K. In both cases temperature formed in the FE part corresponds to the tetragonal phase.

thermal bias the flux reaches $J_- = 2.5$ d.u. and therefore $R_-/R_+ < 1$. This rectification is also characterized by distinct temperature profiles for opposite thermal differences [see Fig. 2(c)].

V. ELECTRIC FIELD EFFECT ON THE MF DIODE

The heat current as a function of Δ is displayed in Fig. 3. We note that the change of the sign of Δ corresponds to the inverted thermal bias. In addition, we consider different amplitudes of the applied electric field in order to see whether an electric field may enhance the heat rectification effect. As shown in Fig. 3(a) the rectification effect becomes stronger upon increasing the electric field strength. However, the role of the electric field is not trivial. As shown in the inset, there is an optimum electric field for which the asymmetry of the diode is maximal. The optimal value $E \approx 0.75$ d.u. corresponds to the frequency-matching condition $\omega_{\rm FM} \approx \omega_{\rm FE}(0) + \Delta\omega_{\rm FE}$ and is quite close to the analytical value that we estimated above without interface ME coupling. Further increasing the electric field destroys the spectra-matching condition and reduces the heat current. Magnetic field B, however, monotonically decreases the heat flux, as shown in Fig. 3(b). This is due to the fact that the stronger the magnetic field is, the stiffer the magnetization is in the FM part, which suppresses the energy transport.

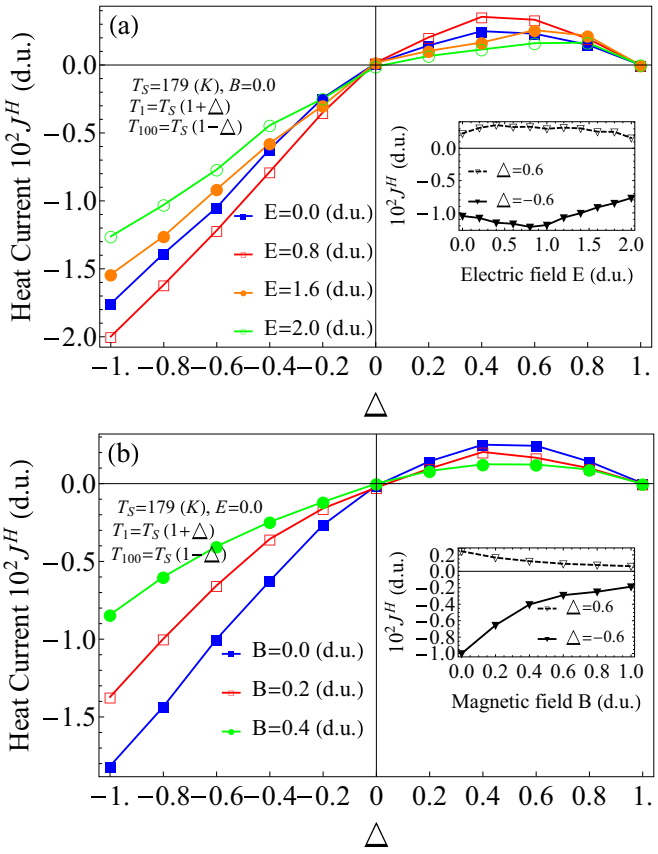

FIG. 3. (Color online) (a) Heat current vs the biased temperature difference in the MF diode for different values of electric field E. The MF diode includes 50 FE cells (from 1 to 50) and 50 FM cells (from 51 to 100). FE-FM coupling coefficients are $g_1 = g_2 = -1$ d.u. Other employed parameters are tabulated in Table I in the Appendix. The inset shows the dependence of heat current on electric field for $\Delta = \pm 0.6$. (b) The same as in (a), but for magnetic field. The electric field increases the heat current, reaching a maximum at the optimal electric field. In contrast, the magnetic field decreases the heat current.

VI. INTERFACIAL ME COUPLING EFFECTS ON THE MF DIODE

Figure 4 shows the heat current as a function of the interfacial ME coupling constant ($g = g_1 = g_2$ d.u.) for forward and reverse biases, respectively. Without magnetoelectric coupling the heat current across the MF diode diminishes. In the range of $g = [-1,0]$ d.u. the rectifying effect is magnified monotonically when increasing g from 0 to -1, and the maximum rectifying effect (asymmetry) is achieved at $g = -1$ d.u., which is the value we have used in all other simulations. Surprisingly, a different picture emerges in the positive range of $g = [0,0.8]$ d.u., where a large coupling strength near 0.8 d.u. deteriorates the heat current in both directions. The optimal transport and rectification are achieved at an intermediate strength of g around 0.4 d.u. This distinct response upon the sign change of the coupling constant can be traced back to the fact that such a change influences the ground state of the polarization and the magnetization configurations of the MF diode system. For a different sign of the coupling constant, slightly different configurations correspond to the

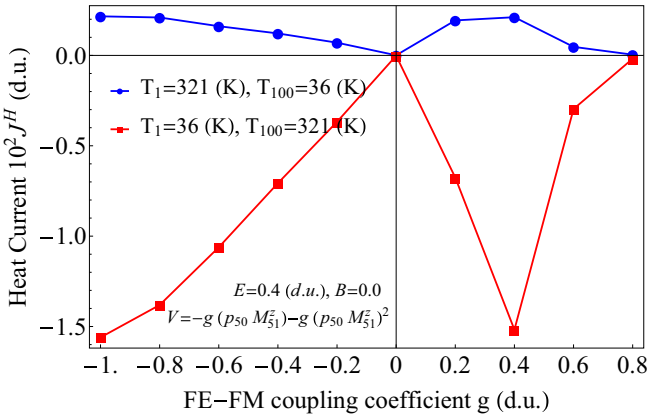

FIG. 4. (Color online) Heat current in the MF diode vs FE-FM coupling coefficients ($g = g_1 = g_2$ d.u.) for forward and reverse temperature biases. The MF diode includes 50 FE cells (from 1 to 50) and 50 FM cells (from 51 to 100). The applied electric and magnetic fields are $E = 0.4$ d.u. and $B = 0.0$ d.u. Other employed parameters are tabulated in Table I in the Appendix.

ground state with a minimal energy. For the explicit form of the interface coupling term $V = -g(P_N M_1^z) - g(P_N M_1^z)^2$ we find that the positive coupling constant $g > 0$ favors large values of the magnetization component M_1^z. Aligning the magnetic moment along the z axis naturally decreases the current, which is consistent with the picture in the inset of Fig. 3(b). In the case of a negative $g < 0$ the situation is different. A small M_1^z means larger transversal components, and this enhances the current.

In summary, we proposed and demonstrated a thermal diode based on a two-phase multiferroic composite. The heat transfer through it can be rectified and controlled by a thermal bias and an electromagnetic field. In particular, the external electric field applied to the ferroelectric part of the multiferroic thermal diode can substantially enhance the heat conductance and the rectification. On the other hand, we found that an applied magnetic field decreases the heat current. We demonstrated and discussed how the interfacial magnetoelectric coupling influences the thermal diode operation in a dynamical way. In view of contemporary advances in engineering composite multiferroic structures, the present findings are potentially interesting for applications, such as elements in thermal switches and thermal memories [33] and thermal management via multifunctional caloric materials [37].

APPENDIX

1. Definitions of the dimensionless units

The total energy of the ferroelectric subsystem H_P as a function of the coarse-grained polarization P_n and corresponding equations of motion read $H_P = \sum_{n=1}^{N} \frac{\alpha_0}{2}\dot{P}_n^2 - \frac{\alpha_1}{2}P_n^2 + \frac{\alpha_2}{4}P_n^4 + \frac{\kappa}{2}(P_{n+1} - P_n)^2 - E P_n$ and $\alpha_0 \ddot{P}_n = \alpha_1 P_n - \alpha_2 P_n^3 - \kappa[-(P_{n+1} - P_n) + (P_n - P_{n-1})] + E$. These equations are normalized by introducing $p_n = P_n/P_0$, $E \to E/kP_0$. Dividing both parts by κ leads to the new reduced time $t'^2 = t^2/(\kappa/\alpha_0)$ or $t' = \omega_0 t$, where $\omega_0 = \sqrt{\frac{\kappa}{\alpha_0}}$. Finally, we obtain the equation for the polarization dynamics in fully dimensionless units for $n \neq N$ [see Eq. (1)] with $\alpha^{\rm FE} = \alpha_1/\kappa$, $\beta^{\rm FE} = \alpha_2 P_0^2/\kappa$.

2. Time scales

The frequency of oscillations associated with the mode-plasma frequency ω_0 is higher than the inverse relaxation time α_1/γ_ν [38] (see Table I). The overdamped case yields the Landau-Khalatnikov equation [39] employed for modeling the polarization hysteresis [22,38]). An overview of the real parameters and their dimensionless counterparts for the ferroelectric subsystem is given in Table I. The time scale within the present calculations is set by the frequency ω_0, which is related to the mode-plasma frequency or the fast oscillations (also known as "eigendisplacements" or Slater modes [30]) of the Ti atom in $BaTiO_3$. *Ab initio* calculations for $BaTiO_3$ [40] yield $\Omega_{\rm Slater} = 1519\,{\rm cm}^{-1} = 286 \times 10^{12}\,{\rm s}^{-1}$; the experimental values differ slightly at $T = 300$ K, yielding $\Omega_{\rm Slater} = 1628\,{\rm cm}^{-1}$, as given in Ref. [41]. Finally, one can also estimate the mode-plasma frequency as [42] $\omega_0 = Z_{\rm Ti}^* e\sqrt{\frac{1}{m_{Ti}\varepsilon_0 a_0^3}}$, where $Z_{\rm Ti}^* = 7$, given in Ref. [21], is the Born effective charge and $m_{Ti} = 47.9$ amu $= 79.5 \times 10^{-27}$ kg. For a displacement of several angstroms, $\omega_0 \approx 100 \times 10^{12}\,{\rm s}^{-1}$. In our numerical calculations the dimensionless time scales, however, with the prefactor of $\omega_0/(2\pi)$; therefore, we arrive at the approximate value of $\sim 10^{12}$ Hz.

3. Parameters of the FM part

For the FM part we employ the Landau-Lifshitz-Gilbert equation of motion [43,44] [(see Eq. (3)]. Bulk parameters for Fe are the anisotropy strength $K_1 \approx 5.0 \times 10^4\,{\rm J/m}^3$ given in Ref. [31] and the saturation magnetization $M_S = 1.7 \times 10^6$ A/m given in Ref. [31]. The Larmor (precessional) frequency in the local anisotropy field scales as $\omega_{\rm prec}/(2\pi) = \gamma 2K_1/(M_S) \approx 8 \times 10^9$ Hz, and the frequency associated with the relaxation scales as $\omega_{\rm rel}/(2\pi) = \alpha_{\rm FM}\omega_{\rm prec}/(2\pi) \approx 0.08 \times 10^9$ Hz. The autocorrelation functions of the thermal fields in the FE and FM parts in standard units are given as $\langle \xi_k(t)\xi_k(t')\rangle = \frac{2k_B\gamma_\nu}{a_{\rm FE}^3} T_k \delta(t - t')$ and $\langle \eta_k^i(t)\eta_k^j(t')\rangle = \frac{2k_B\alpha_{\rm FM}}{\gamma M_S a_{\rm FM}^3} T_k \delta_{kM}\delta_{ij}\delta(t - t')$, where T_k is the site-dependent local temperature in degrees Kelvin.

4. Shift of ferroelectric frequency

We consider one unit cell in the FE Hamiltonian: $H_P = \frac{1}{2}\dot{p}^2 - \frac{\alpha^{\rm FE}}{2}p^2 + \frac{\beta^{\rm FE}}{4}p^4 - Ep$. Equilibrium properties are given by the condition $\partial H_p = 0$. After solving the cubic equation, we obtain $p_1^{(0)} = \frac{2}{\sqrt{3}}\sqrt{\frac{\alpha^{\rm FE}}{\beta^{\rm FE}}}\cos(\frac{\theta}{3})$, $p_2^{(0)} = \frac{2}{\sqrt{3}}\sqrt{\frac{\alpha^{\rm FE}}{\beta^{\rm FE}}}\cos(\frac{\theta}{3} + \frac{2\pi}{3})$, and $p_3^{(0)} = \frac{2}{\sqrt{3}}\sqrt{\frac{\alpha^{\rm FE}}{\beta^{\rm FE}}}\cos(\frac{\theta}{3} + \frac{4\pi}{3})$. Here $\theta = \arccos(\frac{3E}{2\alpha^{\rm FE}}\sqrt{\frac{3\beta^{\rm FE}}{\alpha^{\rm FE}}})$, and the minimum of the energy reads $H(p_{1,2}^{(0)}(E)) = -\frac{(\alpha^{\rm FE})^2}{4\beta^{\rm FE}} \pm \sqrt{\frac{\alpha^{\rm FE}}{\beta^{\rm FE}}}E$. As we can see, if $E > 0$, then the minimum of the energy corresponds to the solution $p_1^{(0)}(E)$, while if $E < 0$, then the energy minimum corresponds to the solution $p_2^{(0)}(E)$. Taking into account the fact that the

system is even in the electric field, we express the minimum of the energy in the form valid for both the $E > 0$ and $E < 0$ cases: $H(p^{(0)}_{1,2}(E)) = -\frac{(\alpha^{\rm FE})^2}{4\beta^{\rm FE}} - \sqrt{\frac{\alpha^{\rm FE}}{\beta^{\rm FE}}}|E|$.

In order to evaluate the dependence of the FE frequency on the applied external electric field we expand the Hamiltonian H_p in the vicinity of the equilibrium points. In the equation of motion governed by the linearized Hamiltonian $\ddot{p} = -(-\alpha^{\rm FE} + 3\beta^{\rm FE}p_0^2)p + E$ enters the electric-field-dependent frequency: $\omega_p^2(E) = (-\alpha^{\rm FE} + 3\beta^{\rm FE}p_0^2)$. Considering the small electric field E in the first-order approximation from $p^{(0)}_{1,2,3}$, we obtain $\omega_p(E > 0) = \sqrt{2\alpha^{\rm FE}} + \frac{3E}{2\alpha^{\rm FE}}\sqrt{\frac{\beta^{\rm FE}}{2}}$, $\omega_p(E < 0) = \sqrt{2\alpha^{\rm FE}} - \frac{3E}{2\alpha^{\rm FE}}\sqrt{\frac{\beta^{\rm FE}}{2}}$, and $\omega_p(E = 0) = \sqrt{2\alpha^{\rm FE}}$. The FE frequency shift due to the applied weak electric field reads $\Delta\omega_p(E) = \omega_p(E) - \omega_p(0) \approx \frac{3|E|}{2\alpha^{\rm FE}}\sqrt{\frac{\beta^{\rm FE}}{2}}$. As we can see, the frequency shift is even in the electric field. On the other hand, the FM frequency is equal to $\omega_D = 2D$. The matching condition between the frequencies ($\omega_D = \omega_p + \Delta\omega_p$) defines the optimum electric field relevant to the maximal conductance: $|E| = |\frac{2\alpha^{\rm FE}}{3}\sqrt{\frac{\alpha^{\rm FE}}{3\beta^{\rm FE}}}\cos[\frac{3}{2}\cos^{-1}(\frac{4D^2-\alpha^{\rm FE}}{2\alpha^{\rm FE}})]|$.

[1] B. Liang, B. Yuan, and J. C. Cheng, Phys. Rev. Lett. **103**, 104301 (2009).

[2] B. Liang, X. Guo, J. Tu, D. Zhang, and J. C. Cheng, Nat. Mater. **9**, 989 (2010); B. Li, *ibid.* **9**, 962 (2010); X.-F. Li, X. Ni, L. Feng, M.-H. Lu, C. He, and Y.-F. Chen, Phys. Rev. Lett. **106**, 084301 (2011); M. Maldovan, Nature (London) **503**, 209 (2013).

[3] J. Ren, Phys. Rev. B **88**, 220406(R) (2013); J. Ren and J.-X. Zhu, *ibid.* **88**, 094427 (2013); J. Ren, J. Fransson, and J.-X. Zhu, *ibid.* **89**, 214407 (2014)

[4] S. Lepri, R. Livi, and A. Politi, Phys. Rev. Lett. **78**, 1896 (1997); T. S. Komatsu and N. Ito, Phys. Rev. E **83**, 012104 (2011); T. S. Komatsu and N. Nakagawa, *ibid.* **73**, 065107(R) (2006).

[5] P. Kim, L. Shi, A. Majumdar, and P. L. McEuen, Phys. Rev. Lett. **87**, 215502 (2001); W. Kobayashi, Y. Teraoka, and I. Terasaki, Appl. Phys. Lett. **95**, 171905 (2009); B. Li, J. H. Lan, and L. Wang, Phys. Rev. Lett. **95**, 104302 (2005).

[6] M. Terraneo, M. Peyrard, and G. Casati, Phys. Rev. Lett. **88**, 094302 (2002); G. Casati, Chaos **15**, 015120 (2005).

[7] B. Li, L. Wang, and G. Casati, Phys. Rev. Lett. **93**, 184301 (2004); B. Hu, L. Yang, and Y. Zhang, *ibid.* **97**, 124302 (2006).

[8] N. Li, J. Ren, L. Wang, G. Zhang, P. Hänggi, and B. Li, Rev. Mod. Phys. **84**, 1045 (2012).

[9] W. Eerenstein, N. D. Mathur, and J. F. Scott, Nature (London) **442**, 759 (2006); Y. Tokura and S. Seki, Adv. Mater. **22**, 1554 (2010); C. A. F. Vaz, J. Hoffman, Ch. H. Ahn, and R. Ramesh, *ibid.* **22**, 2900 (2010); F. Zavaliche, T. Zhao, H. Zheng, F. Straub, M. P. Cruz, P.-L. Yang, D. Hao, and R. Ramesh, Nano Lett. **7**, 1586 (2007).

[10] H. L. Meyerheim, F. Klimenta, A. Ernst, K. Mohseni, S. Ostanin, M. Fechner, S. Parihar, I. V. Maznichenko, I. Mertig, and J. Kirschner, Phys. Rev. Lett. **106**, 087203 (2011); R. Ramesh and N. A. Spaldin, Nat. Mater. **6**, 21 (2007).

[11] M. Bibes and A. Barthelemy, Nat. Mater. **7**, 425 (2008); M. Gajek, M. Bibe, S. Fusil, K. Bouzehouane, J. Fontcuberta, A. Barthelemy, and A. Fert, *ibid.* **6**, 296 (2007).

[12] D. Pantel, S. Goetze, D. Hesse, and M. Alexe, Nat. Mater. **11**, 289 (2012); C.-W. Nan, M. I. Bichurin, S. Dong, D. Viehland, and G. Srinivasan, J. Appl. Phys. **103**, 031101 (2008).

[13] N. Spaldin and M. Fiebig, Science **309**, 391 (2005); M. Fiebig, J. Phys. D **38**, R123 (2005).

[14] C.-G. Duan, S. S. Jaswal, and E. Y. Tsymbal, Phys. Rev. Lett. **97**, 047201 (2006).

[15] M. Fechner, I. V. Maznichenko, S. Ostanin, A. Ernst, J. Henk, and I. Mertig, Phys. Status Solidi B **247**, 1600 (2010).

[16] M. Mostovoy, Phys. Rev. Lett. **96**, 067601 (2006); H. Katsura, N. Nagaosa, and A. V. Balatsky, *ibid.* **95**, 057205 (2005); S. Park, Y. J. Choi, C. L. Zhang, and S-W. Cheong, *ibid.* **98**, 057601 (2007).

[17] M. Azimi, L. Chotorlishvili, S. K. Mishra, T. Vekua, W. Hübner, and J. Berakdar, New J. Phys. **16**, 063018 (2014).

[18] M. Azimi, L. Chotorlishvili, S. K. Mishra, S. Greschner, T. Vekua, and J. Berakdar, Phys. Rev. B **89**, 024424 (2014).

[19] S. Sahoo, S. Polisetty, C.-G. Duan, S. S. Jaswal, E. Y. Tsymbal, and C. Binek, Phys. Rev. B **76**, 092108 (2007).

[20] J. Lee, N. Sai, T. Cai, Q. Niu, and A. A. Demkov, Phys. Rev. B **81**, 144425 (2010).

[21] *Physics of Ferroelectrics*, edited by K. Rabe, Ch. H. Ahn, and J.-M. Triscone (Springer, Berlin, 2007).

[22] A. Picinin, M. H. Lente, J. A. Eiras, and J. P. Rino, Phys. Rev. B **69**, 064117 (2004).

[23] J. J. Wang, P. P. Wu, X. Q. Ma, and L. Q. Chen1, J. Appl. Phys. **108**, 114105 (2010).

[24] O. E. Fesenko and V. S. Popov, Ferroelectrics **37**, 729 (1981).

[25] C. Hess, P. Ribeiro, B. Büchner, H. ElHaes, G. Roth, U. Ammerahl, and A. Revcolevschi, Phys. Rev. B **73**, 104407 (2006); C. Hess, H. ElHaes, A. Waske, B. Büchner, C. Sekar, G. Krabbes, F. Heidrich-Meisner, and W. Brenig, Phys. Rev. Lett. **98**, 027201 (2007).

[26] J. Xiao, G. E. W. Bauer, K.-c. Uchida, E. Saitoh, and S. Maekawa, Phys. Rev. B **81**, 214418 (2010); K. I. Uchida, T. Kikkawa, A. Miura, J. Shiomi, and E. Saitoh, Phys. Rev. X **4**, 041023 (2014).

[27] C.-L. Jia, T.-L. Wei, C.-J. Jiang, D.-S. Xue, A. Sukhov, and J. Berakdar, Phys. Rev. B **90**, 054423 (2014); A. Sukhov, C.-L. Jia, L. Chotorlishvili, P. P. Horley, D. Sander, and J. Berakdar, *ibid.* **90**, 224428 (2014); N. Jedrecy, H. J. von Bardeleben, V. Badjeck, D. Demaille, D. Stanescu, H. Magnan, and A. Barbier, *ibid.* **88**, 121409(R) (2013); T. Nan *et al.*, Sci. Rep. **4**, 3688 (2014); C.-L. Jia, F. Wang, C.-J. Jiang, J. Berakdar, and D.-S. Xue, *ibid.* **5**, 11111 (2015).

[28] L. Chotorlishvili, Z. Toklikishvili, V. K. Dugaev, J. Barnas, S. Trimper, and J. Berakdar, Phys. Rev. B **88**, 144429 (2013).

[29] S. R. Etesami, L. Chotorlishvili, A. Sukhov, and J. Berakdar, Phys. Rev. B **90**, 014410 (2014).

[30] J. Hlinka and P. Marton, Phys. Rev. B **74**, 104104 (2006); P. Marton and J. Hlinka, Ferroelectrics **373**, 139 (2008); N.

Setter, D. Damjanovic, L. Eng, G. Fox, S. Gevorgian, S. Hong, A. Kingon, H. Kohlstedt, N. Y. Park, G. B. Stephenson, I. Stolichnov, A. K. Tagantsev, D. V. Taylor, and T. Yamada, J. Appl. Phys. **100**, 051606 (2006); S. Sivasubramanian, A. Widom, and Y. N. Srivastava, Ferroelectrics **300**, 43 (2004).

[31] J. M. D. Coey, *Magnetism and Magnetic Materials* (Cambridge University Press, Cambridge, 2010).

[32] A. Klümper and K. Sakai, J. Phys. A **35**, 2173 (2002).

[33] S. Li, X. Ding, J. Ren, X. Moya, J. Li, J. Sun, and E. K. H. Salje, Sci. Rep. **4**, 6375 (2014).

[34] L. Chotorlishvili, R. Khomeriki, A. Sukhov, S. Ruffo, and J. Berakdar, Phys. Rev. Lett. **111**, 117202 (2013).

[35] S. Nambu and D. A. Sagala, Phys. Rev. B **50**, 5838 (1994); E. Klotins, Ferroelectrics **370**, 184 (2008).

[36] D. Viehland and Y. H. Chen, J. Appl. Phys. **88**, 6696 (2000).

[37] X. Moya, S. Kar-Narayan, and N. D. Mathur, Nat. Mater. **13**, 439 (2014).

[38] D. Ricinschi, C. Harnagea, C. Papusoi, L. Mitoseriu, V. Tura, and M. Okuyama, J. Phys. Condens. Matter **10**, 477 (1998).

[39] L. D. Landau and I. M. Khalatnikov, Dokl. Akad. Nauk SSSR **96**, 469 (1954).

[40] Ph. Ghosez, E. Cockayne, U. V. Waghmare, and K. M. Rabe, Phys. Rev. B **60**, 836 (1999).

[41] J. L. Servoin, F. Gervais, A. M. Quittet, and Y. Luspin, Phys. Rev. B **21**, 2038 (1980).

[42] W. Cao, J. Phys. Soc. Jpn. **63**, 1156 (1994).

[43] L. D. Landau and E. M. Lifshitz, Phys. Z. Sowjetunion **8**, 153 (1935).

[44] T. L. Gilbert, Phys. Rev. **100**, 1243 (1955); IEEE Trans. Magn. **40**, 3443 (2004).

[45] J. L. Doman, D. Fiorani, and E. Tronc, Adv. Chem. Phys. **98**, 283 (1997).

[46] J. Hlinka, J. Petzelt, S. Kamba, D. Noujni, and T. Ostapchuk, Phase Transitions **79**, 41 (2006).